



Fracture behaviour of concrete with different replacement rates of iron tailings sand based on double-K criterion

Yao Zhang, Wei-Hua Ma, Hong-Zhen Kang, Qiang Li

School of Civil Engineering, Tangshan University, Tangshan 063000, China; Hebei Key Laboratory of Building Engineering and Tailings Utilization, Hebei Tangshan 063000, China.

zhangyao@tsc.edu.cn, 1195794977@qq.com, 375860802@qq.com, 281543170@qq.com



ABSTRACT. The article conducts a study on the iron tailings sand concrete's fracture behaviour based on the double-K criterion. Five sets of three-point bending beam specimens (100×150×700 mm) of concrete with 0%, 25%, 50%, 75% and 100% (mass ratio) iron tailings sand replacement river sand respectively were fracture tested, and the P-CMOD and P- ϵ curves of each set of specimens were measured to determine the initial cracking load (P_{ini}), unstable cracking load (P_{max}), initial cracking toughness (K_{IC}^{ini}) and unstable cracking toughness (K_{IC}^{un}). After the fracture test, samples were extracted from the specimens and subjected to scanning electron microscopy (SEM) and mercury intrusion porosimetry (MIP) for microscopic analysis. Macroscopic test results: by comparing the variation pattern of P-CMOD curve and observing the fracture percentage of coarse aggregate in the section, it is found that the fracture processes and damage patterns of iron tailings sand concrete and river sand concrete are comparable; by comparing P_{ini} , P_{max} , K_{IC}^{ini} , K_{IC}^{un} , it is founded that the addition of iron tailings sand improves initial cracking load and initial cracking toughness more significantly than unstable cracking load and unstable cracking toughness; by comparing P_{ini} / P_{max} , and $K_{IC}^{ini} / K_{IC}^{un}$, it is founded that the ductility of iron tailings sand concrete is marginally inferior. Microscopic test results: the SEM images show that the interface transition zone (ITZ) of iron tailings sand concrete is denser and the bonding state is better, and the MIP show that the addition of iron tailings sand can refine the pore size, reduce large pores and increase small pores. Therefore, from the assessment of fracture mechanics, iron tailings sand can totally replace river sand in equivalent quantities for concrete preparation, which will provide great potential for the secondary use of iron tailings sand.

Citation: Zhang, Y., Ma, W. H., Kang, H. Z., Li, Q., Fracture behaviour of concrete with different replacement rates of iron tailings sand based on double-K criterions, *Frattura ed Integrità Strutturale*, 64 (2023) 171-185.

Received: 05.12.2022

Accepted: 31.01.2023

Online first: 18.02.2023

Published: 01.04.2023

Copyright: © 2023 This is an open access article under the terms of the CC-BY 4.0, which permits unrestricted use, distribution, and reproduction in any medium, provided the original author and source are credited.

KEYWORDS. Iron tailings sand concrete, Double-K criterion, Replacement rate, Three-point bending beam, Microscopic test.

INTRODUCTION

As the largest building material, the production of concrete inevitably consumes large amounts of sand and gravel raw materials [1]. However, the problem of the increasing cost and tight supply of high-quality natural sand is becoming more pronounced, and the search for resources that can replace natural sand is of profound significance in solving the environmental and social problems caused by sand mining. As the iron and steel sector expands quickly, emissions of industrial waste iron tailings sand from ore dressing rise year over year, yet only 20% of iron tailings sand is recycled as resource [2]. Storage of the remaining tailings requires the construction of a tailings pond, which not only poses the risk of collapse and landslides but also causes serious environmental pollution due to seepage of hazardous substances from the tailings [3]. As a result, the secondary use of iron tailings sand has received attention and research from countries around the world. Similar to the nature of natural aggregates, iron tailings sand consists primarily of silica, alumina, iron, magnesium, and calcium [4]. The production of concrete using iron tailings sand as a partial or total replacement for river sand has become one of the most common uses for transforming iron tailings sand into an engineering material. This will not only alleviate the pressure on the concrete industry caused by the lack of natural sand and reduce construction costs significantly, but it will also reduce the environmental and social risks associated with iron tailings sand, thereby contributing to the achievement of sustainable development through an efficient and environmentally friendly production process.

In recent years, both domestic and international researchers have made advances in the manufacture and performance testing of iron tailings sand concrete [5-10]. Liu et al. [5] prepared shotcrete by replacing natural sand with iron tailings sand in equal proportions; following a series of tests, iron tailings sand concrete that met the required strength and engineering specifications was obtained. Zhang et al. [6] blended iron tailings sand with manufactured sand to produce high-performance concrete with good workability. When the iron tailings sand percentage was between 20% and 40%, the compressive strength was found to be higher than that of concrete made with just river sand. In particular, when the replacement rate was 20%, the compressive strength at 28 days of age is 14% more than that of concrete containing pure river sand, and longer age or more admixture reduces this percentage. Shettima et al. [7] produced concrete with different replacement rates of iron tailings sand and discovered that, compared to conventional concrete, concrete containing iron tailings sand had higher compressive and, splitting tensile strengths and modulus of elasticity, but poorer compatibility, lower drying shrinkage, depth of carbonation, increased water absorption and chloride ion permeability with increasing iron tailings sand content. Tian et al. [8] evaluated the concrete with different dosing levels of iron tailings sand based on workability and mechanical properties and determined the optimal replacement rate to be 35%. Chinnappa et al. [9] tested the mechanical properties of concrete with different replacement rates of iron tailings sand and established a regression model that was statistically significant and validated by comparing measured values. The test results showed that for different water-cement ratios, the increase in compressive strength, splitting tensile strength, and flexural strength of concrete with IOT-alccofine were observed to increase. However, the IOT replacement levels to reach the maximal strength was varied for various water-cement ratios. Zhu [10] discusses the viability of using iron tailings sand to produce ultra-high performance concrete. An investigation was conducted into the impacts of fine aggregate type, replacement ratio, and maximum particle size on its performance. The results indicated that UHPC performs best when 60% of silica sand was substituted with 0-1.18 mm IOT as mixed fine aggregate, which was superior to employing silica sand alone as aggregate. Using scanning electron microscopy, the interfacial transition zone was observed to show the mechanism of the effect of micro powder content in iron tailing sand on strength.

The majority of studies on iron tailings sand concrete have focused on its mechanical properties, workability and durability, with little research reported on its fracture behaviour. However, similar to concrete materials, iron tailings sand concrete is highly susceptible to cracking due to its low tensile strength and crack resistance [11]. After cracking, it is difficult to prevent the erosion of materials by dangerous chemicals, which, in mild situations, can disrupt the regular usage of the building and, in severe circumstances, can risk the entire structure's safety [12]. Fracture mechanics is the study of the strength and propagation of cracks in cracked objects. It is one of the most essential tools in structural design and plays an increasingly important role in material selection and process design. Citing reasonable concrete fracture guidelines and seeking testing techniques that are both theoretical and operable are key to exploring the fracture characteristics of iron tailings sand concrete structures and determining their fracture parameters. The double-K fracture model [13, 14] proposed by Chinese scholars Xu and Reinhardt is effective in predicting crack initiation, stable extension and unstable extension. The model combines the fictitious crack concept reflecting the softening characteristics of concrete with the stress intensity factor at the tip of the notch. In recent years, domestic and international academics have conducted a large number of studies and researches in the specimen form [15, 16], calculating methods [17-20], influencing factors [21-23] theoretical extensions and applications [24-27].

Given that the fracture behavior of iron tailings sand concrete has not been investigated, the influence of its replacement rate on its fracture properties is also unclear. The article investigates the fracture characteristics of iron tailings sand concrete at different replacement rates based on the double-K fracture model of concrete, using macroscopic tests on three-point bending beams and microscopic testing techniques such as scanning electron microscopy. The findings will provide a scientific basis for deciding whether iron tailings sand concrete may be utilized safely in engineering.

EXPERIMENTAL OVERVIEW

Materials and Mix Proportions

For this study, PO42.5 regular Portland cement, ordinary mineral powder, and primary grade fly ash were used. The particle size range of 5–10 mm accounted for 35% of the coarse aggregate, while the particle size range of 10–20 mm accounted for 65%. The fine aggregate was river sand and iron tailings sand which was supplied by a Qian'an, Hebei-based mining company. Tab. 1 presents the chemical composition of iron tailings sand which was determined by X-Ray fluorescence (XRF) method. Measuring according to JGJ52-2006 [28], the test data showed that the river sand had: fineness modulus = 2.54, apparent density = 2550kg/m³, and water absorption rate = 2.78%, and the iron tailings sand had: fineness modulus = 2.11, apparent density = 2740kg/m³, and water absorption rate = 3.63%. The grain size distributions of the iron tailings sand and river sand are shown in Fig. 1. Polycarboxylic high-performance water-reducing agent was added, and tap water was mixed with. All samples were named with letters and numbers. The first group, designated S0, consisted of river sand without iron tailings sand. In the other four mixtures, river sand was replaced with iron tailings sand at proportions of 25%, 50%, 75%, and 100% by mass; these mixtures were designated S1, S2, S3, and S4 accordingly. The proportions of the five mixtures are detailed in Tab. 2.

Composition	SiO ₂	K ₂ O	Na ₂ O	MgO	Al ₂ O ₃	TiO ₂	Fe ₂ O ₃	CaO	SO ₃	Other
Weight/%	71.8	1.1	1.1	3.7	4.5	0.3	13.1	2.8	0.4	1.2

Table 1: Chemical compositions of the iron tailing sand.

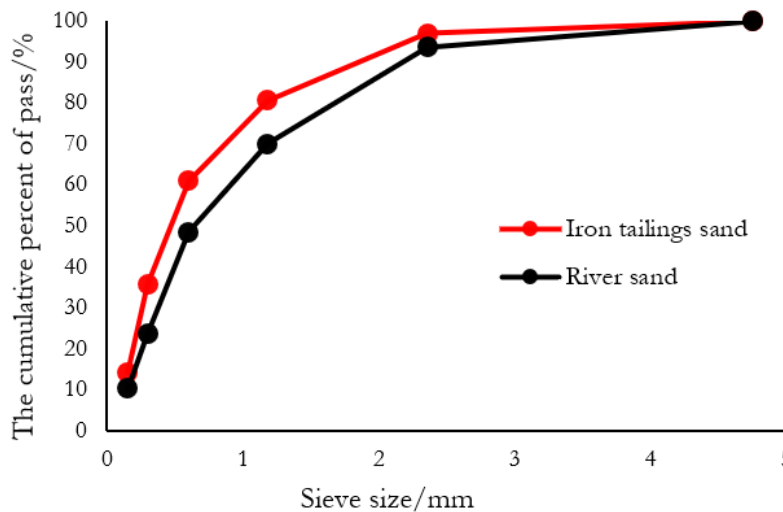


Figure 1: Grain size distributions of sands.

Specimen preparation

Fig. 2 depicts the form of the three-point bending beam. Five groups of four specimens were cast, however owing to faulty manufacture, handling, and testing, some groups included fewer than four specimens. Simultaneously, three 100mm × 100mm × 100mm cube specimens were created for each group in order to evaluate the compressive strength [29].

Before the concrete was poured, a 2 mm thick steel plate with oily release agent-coated sides was put into the test mold to generate a precast notch. After being poured, the specimens were left for three days at 25 ± 5°C, after which the mold was removed and the specimens were numbered. After 28 days of sprinkling water curing, the specimens were maintained

naturally for 1,520 days until the fracture test.

Group	Water binder ratio	Material utilization amount /kg/m ³								Average cubic compressive strength /MPa
		Cement	River sand	Coarse aggregate	Water	Iron tailings sand	Fly ash	Mineral powder	Water-reducing agent	
S0	0.483	191	815	1118	142	/	31	72	1.56	38.43(2.67)
S1	0.517	191	611.3	1118	152	203.7	31	72	1.56	37.87(2.15)
S2	0.544	191	407.5	1118	160	407.5	31	72	1.56	41.52(1.52)
S3	0.554	191	203.7	1118	163	611.3	31	72	1.56	41.66(2.31)
S4	0.578	191	/	1118	170	815	31	72	1.56	44.17(2.01)

Table 2: Mixture proportions of concrete and compressive strength (standard deviations in parentheses).

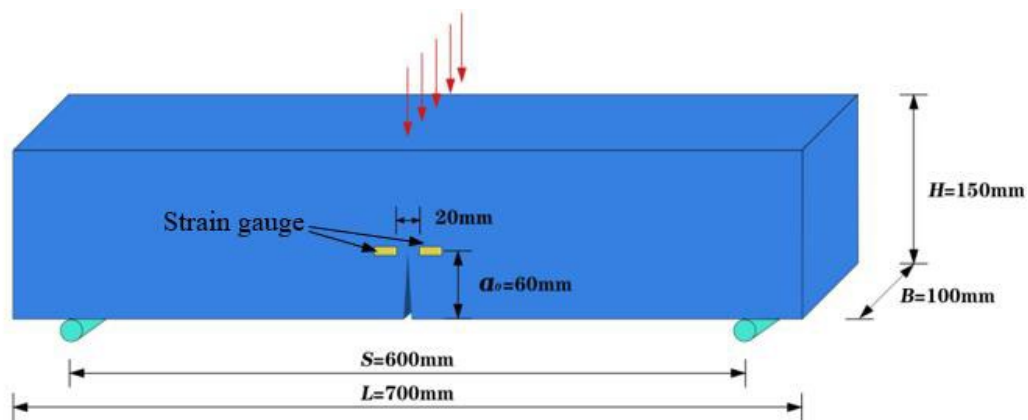


Figure 2: Sketch of three-point bending beam.

Test procedure - Macroscopic tests

The cube compressive strength of concrete was measured and the resultant average strength is shown in Tab. 2. As can be seen from Tab. 2, the average cubic compressive strength after admixing iron tailings sand was higher than that of river sand concrete, with a maximum increase of 15%, except for the specimen with a 25% replacement rate. The three-point bending beam test was performed according to DL/T5332-2005 [30] by a 100 kN-ranged electronic universal testing machine, and the testing setup is depicted in Fig. 3. The load sensor of testing machine measured the load with an accuracy of 1%. The crack mouth opening displacement (CMOD) was measured using a 4mm clip gauge, which was mounted at the notch of the bottom. The specimen was supported by a customized brace to prevent the dislodged clip gauge from being crushed by the specimen in the event of a fracture. To estimate the initial cracking load (P_{ini}), strain gauges with a standard distance of 20 mm were attached symmetrically at 10 mm on either side of the center of the notch. The bridge connection of the measurement points was a quarter bridge considering temperature compensation. The DH3820 static acquisition system was utilized to record the load, strain and crack opening displacement (CMOD). The load sensor and clip gauge were calibrated before to the test. The test was conducted at a displacement rate of 0.05 mm/min for continuous loading until the specimen cracked, and data were collected at a frequency of 10 HZ.

Test procedure - Microscopic tests

In order to investigate the hydration products and the microscopic morphology of the interfacial transition zone (ITZ), an approximately 10 mm × 10 mm × 10 mm specimen was sliced at the fracture surface using a cutter after the three-point bending beam test. The specimen was placed in the apparatus to remove the vacuum and spray gold over the surface of the observation site. The processed specimen was placed in the SEM system (JSM7900F) and parameters such as voltage, current, sharpness, magnification, and focal length were adjusted such that the morphology of the investigated location could be observed with clarity.

Each specimen's pore structure was determined using mercury intrusion porosimetry (MIP) (AutoPore V9620, pore size range: 3 nm-1100 μm). After the three-point beam bending test, samples were drilled from the fracture surface. After cleaning, drying, and vacuuming the specimens, they were shattered into 4-5 mm pieces for mercury intrusion porosimetry testing, and the resulting signals were collected to determine porosity and pore size distribution.

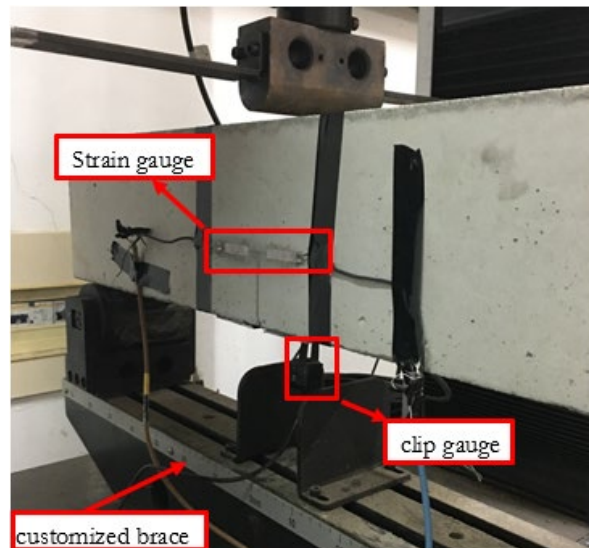


Figure 3: Testing apparatus.

MACROSCOPIC TEST RESULTS AND DISCUSSION

Destruction processes and patterns

The fracture process and damage morphology of concrete with different replacement rates of iron tailings sand did not change appreciably. At the early stage of loading, the crack mouth opening displacement (CMOD) basically increased linearly with the increase of load. After achieving the initial cracking load (P_{ini}), the rate of rise of CMOD improved dramatically, and the curve exhibited non-linear features; nonetheless, the specimen had not yet developed visible fractures. Tiny cracks first emerged at the tip of the prefabricated notch before the unstable cracking load (P_{max}), after which the load decreased and the fractures proceeded to bend and spread upwards until the specimen fractured. Fig. 4 shows the load to crack mouth opening displacement (P-CMOD) curves for several of the specimens recorded by the three-point bending beam test. The specimens chosen were those in each group whose unstable cracking loads (P_{max}) were closest to the group average. As shown in Fig. 4, P_{max} of iron tailings sand concrete was generally higher than that of river sand concrete, but the peak of the curve was narrower, indicating that iron tailings sand concrete was more brittle than ordinary concrete. The morphology of several of these specimens after fracture damage is shown in Fig. 5, with the percentages reflecting the fraction of fractured coarse aggregate in the section relative to the overall coarse aggregate. The fracture percentage of coarse aggregate for river sand concrete and iron tailings sand concrete was typically between 50 and 60 percent, with little difference. The slightly enhanced fracture rate of the iron tailings sand concrete suggested that the inclusion of iron tailings sand increased the strength of the coarse aggregate-mortar interface. Thus, the fractures were more likely to penetrate the coarse aggregate than the aggregate-mortar contact.

Initial cracking load (P_{ini})

Early in the loading process, the strain (ϵ) rose linearly with the load (P). Due to the significant stress concentration at the tip of the precast notch, cracking will occur when the load is increased to a particular level and the concrete energy is released, resulting in a reduction of the strain value near the notch's tip. P_{ini} corresponds to the load corresponding to the point of retraction [31]. Fig. 6 depicts the load-strain (P- ϵ) curves for several of the specimens recorded by the three-point bending beam test. Tab. 3 provides information on P_{ini} of each specimen.

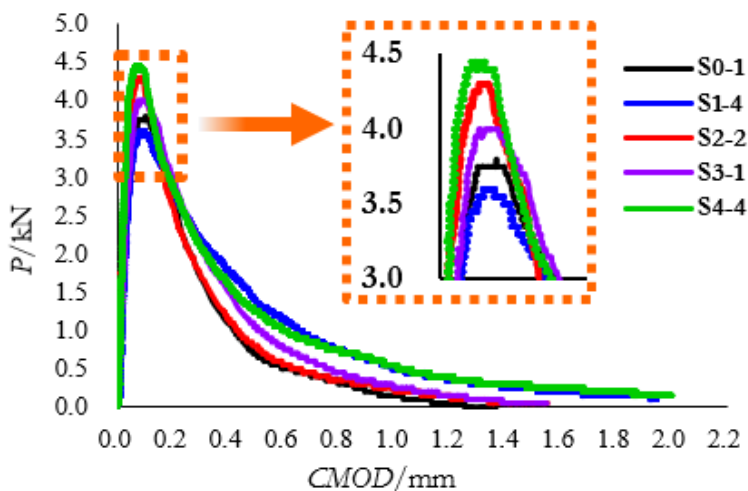


Figure 4: P-CMOD curves of some specimens

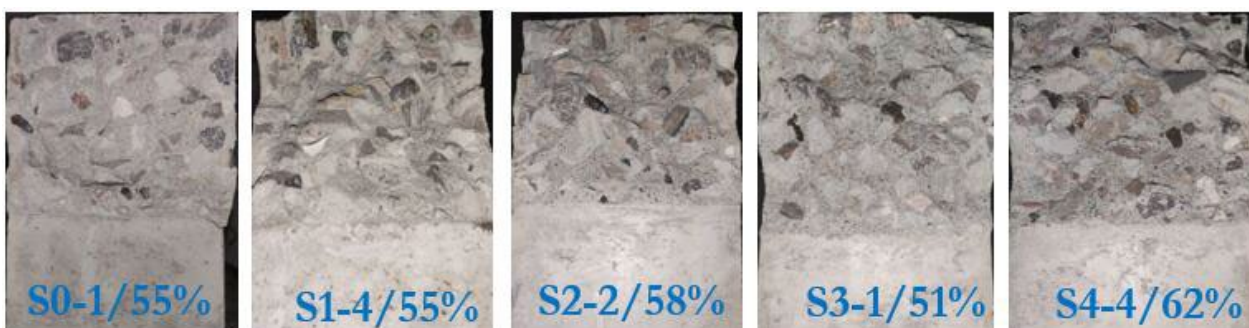


Figure 5: Typical fracture cross section of three-point bending beams.

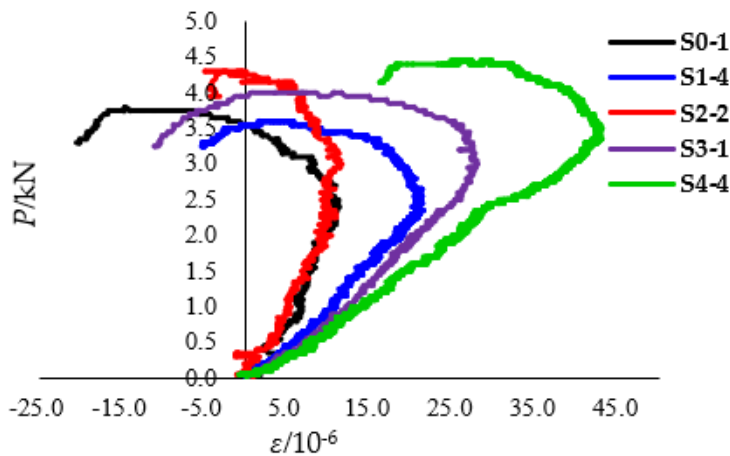


Figure 6: P-ε curves of some specimens

Initial cracking toughness (K_{IC}^{ini}) and *unstable cracking toughness* (K_{IC}^{un})

The initial cracking toughness (K_{IC}^{ini}) can be calculated by bringing the test measured P_{ini} and the initial notch crack length (a_0) into our current regulations [30]:

$$K_I = \frac{3(P+mg/2)S}{2H^2B} \sqrt{a} F_1 \left(\frac{a}{H} \right) \tag{1}$$



$$F_1\left(\frac{a}{H}\right) = \frac{1.99 - \frac{a}{H} \left(1 - \frac{a}{H}\right) \left[\left(2.15 - 3.93 \frac{a}{H} + 2.7 \left(\frac{a}{H}\right)^2\right) \right]}{\left(1 + 2 \frac{a}{H}\right) \left(1 - \frac{a}{H}\right)^{3/2}} \quad (2)$$

where:

K_I : fracture toughness;

P : concentrated load in the span;

mg : mass between the specimen supports (converted from the total mass of the specimen by the S/L ratio, L being the total length of the specimen);

g : gravitational acceleration;

S : the span between the two supports of the specimen;

H : height of the specimen cross-section;

B : thickness of the specimen cross-section;

a : effective crack length;

Sample	P_{ini} /kN	P_{max} /kN	P_{ini} / P_{max}	a_c /mm	K_{IC}^{ini} /MPa·m ^{1/2}	K_{IC}^{un} /MPa·m ^{1/2}	$K_{IC}^{un} - K_{IC}^{ini}$ / MPa·m ^{1/2}	$K_{IC}^{ini} / K_{IC}^{un}$
S0-1	2.40	3.80	0.63	79	0.514	1.176	0.662	0.50
S0-3	2.85	4.35	0.66	75	0.606	1.235	0.629	0.44
S0-4	2.20	3.55	0.62	70	0.473	0.906	0.433	0.46
Average	2.48(0.27)	3.90(0.33)	0.64(0.02)	75(3.68)	0.531(0.056)	1.106(0.143)	0.575(0.101)	0.48(0.02)
S1-1	2.40	3.45	0.70	80	0.514	1.101	0.587	0.45
S1-2	2.75	3.35	0.82	80	0.586	1.050	0.464	0.56
S1-3	3.30	4.05	0.81	71	0.698	1.047	0.349	0.67
S1-4	2.45	3.60	0.68	77	0.524	1.061	0.537	0.49
Average	2.73(0.36)	3.61(0.27)	0.75(0.06)	77(3.67)	0.581(0.073)	1.065(0.022)	0.484(0.090)	0.54(0.08)
S2-1	2.55	4.15	0.61	74	0.545	1.147	0.602	0.48
S2-2	3.00	4.30	0.70	81	0.637	1.381	0.744	0.46
S2-4	3.30	4.30	0.77	76	0.698	1.242	0.544	0.56
Average	2.95(0.31)	4.25(0.07)	0.69(0.07)	77(2.94)	0.627(0.063)	1.257(0.096)	0.630(0.084)	0.50(0.04)
S3-1	3.00	4.00	0.75	80	0.637	1.254	0.617	0.51
S3-2	3.10	4.25	0.73	88	0.658	1.602	0.944	0.41
S3-3	3.05	3.70	0.82	75	0.647	1.059	0.412	0.61
S3-4	2.95	3.75	0.79	84	0.627	1.296	0.669	0.48
Average	3.03(0.06)	3.93(0.22)	0.77(0.03)	81(4.82)	0.642 (0.012)	1.303(0.195)	0.661(0.190)	0.50(0.07)
S4-2	2.90	4.80	0.60	80	0.617	1.512	0.895	0.41
S4-3	3.20	4.25	0.75	75	0.678	1.197	0.519	0.57
S4-4	3.40	4.45	0.76	76	0.719	1.275	0.556	0.56
Average	3.17(0.21)	4.50(0.23)	0.71(0.07)	77(2.16)	0.671(0.042)	1.328(0.134)	0.657(0.169)	0.51(0.07)

Table 3: Double-K fracture parameters of specimens (standard deviations in parentheses).

The unstable cracking load (P_{max}) and the critical effective crack length (a_c) are substituted for P_{ini} and a_0 respectively in Eqn. (1) and (2) to obtain the unstable cracking toughness (K_{IC}^{un}). a_c can be obtained by bringing P_{max} and the corresponding crack mouth opening displacement ($CMOD_c$) into Eqn. (3) based on the principle of linear superposition:

$$a_c = \frac{2}{\pi} (H + H_0) \tan^{-1} \sqrt{\frac{BE}{32.6P_{max}} CMOD_c - 0.1135 - H_0} \tag{3}$$

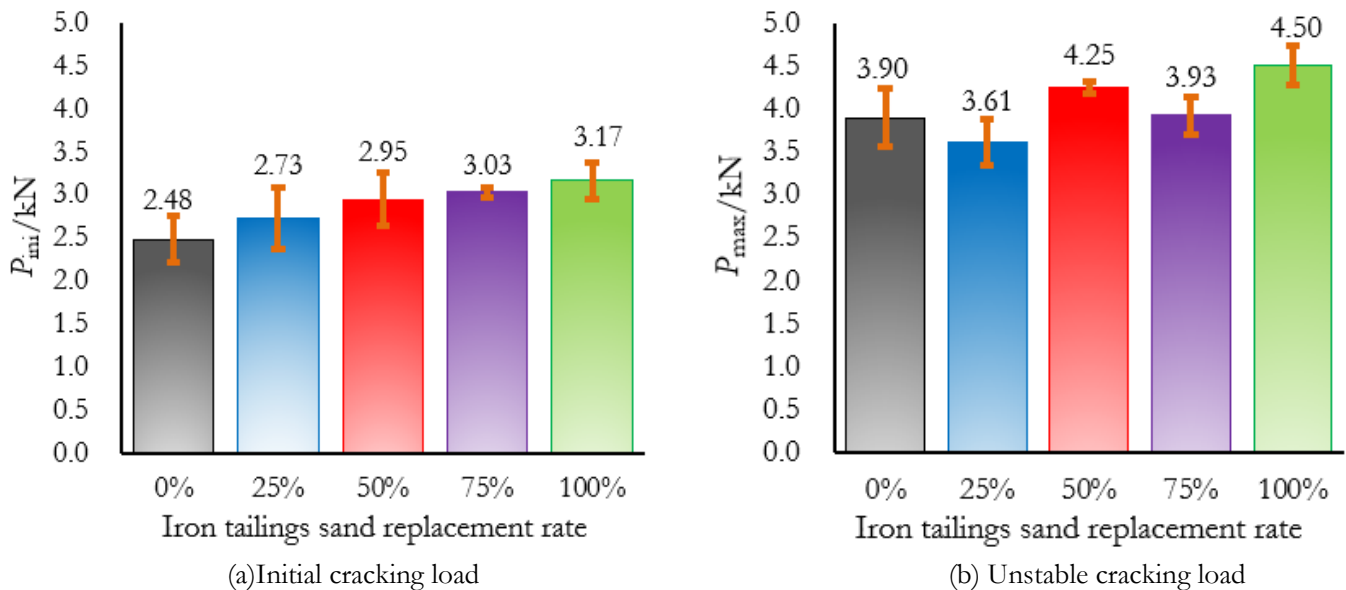
where H_0 is the thickness of holder of clip gauge, E is the calculated Young's modulus and is obtained from the following equation.

$$E = \frac{1}{Bc_i} \left[3.70 + 32.60 \tan^2 \left(\frac{\pi a_0 + H_0}{2 H + H_0} \right) \right] \tag{4}$$

The initial flexibility $c_i = CMOD_i / P_i$, which can be found according to $CMOD_i$ and P_i of any point from the straight line segment of the curve P-CMOD. The results of the fracture parameters obtained according to the above method are listed in Tab. 3.

Discussion of fracture parameters

The variation of each fracture parameter (mean value) with iron tailings sand replacement rate is given in Fig. 7. As can be seen from Fig. 7a, P_{ini} rose by around 28% from 2.48kN for river sand concrete to 3.17kN for concrete with 100% iron tailings sand replacement. P_{max} (Fig. 7b) did not increase monotonically with increasing replacement rate, and decreased from the previous replacement rate at 25% and 75%, but this decrease was not statistically significant. Overall, P_{max} of the specimens with iron tailings sand was not substantially lower than river sand concrete, and P_{max} of the concrete specimens with 100% replacement of iron tailings sand increased by 15% compared to that of river sand concrete, which was lower than P_{ini} .



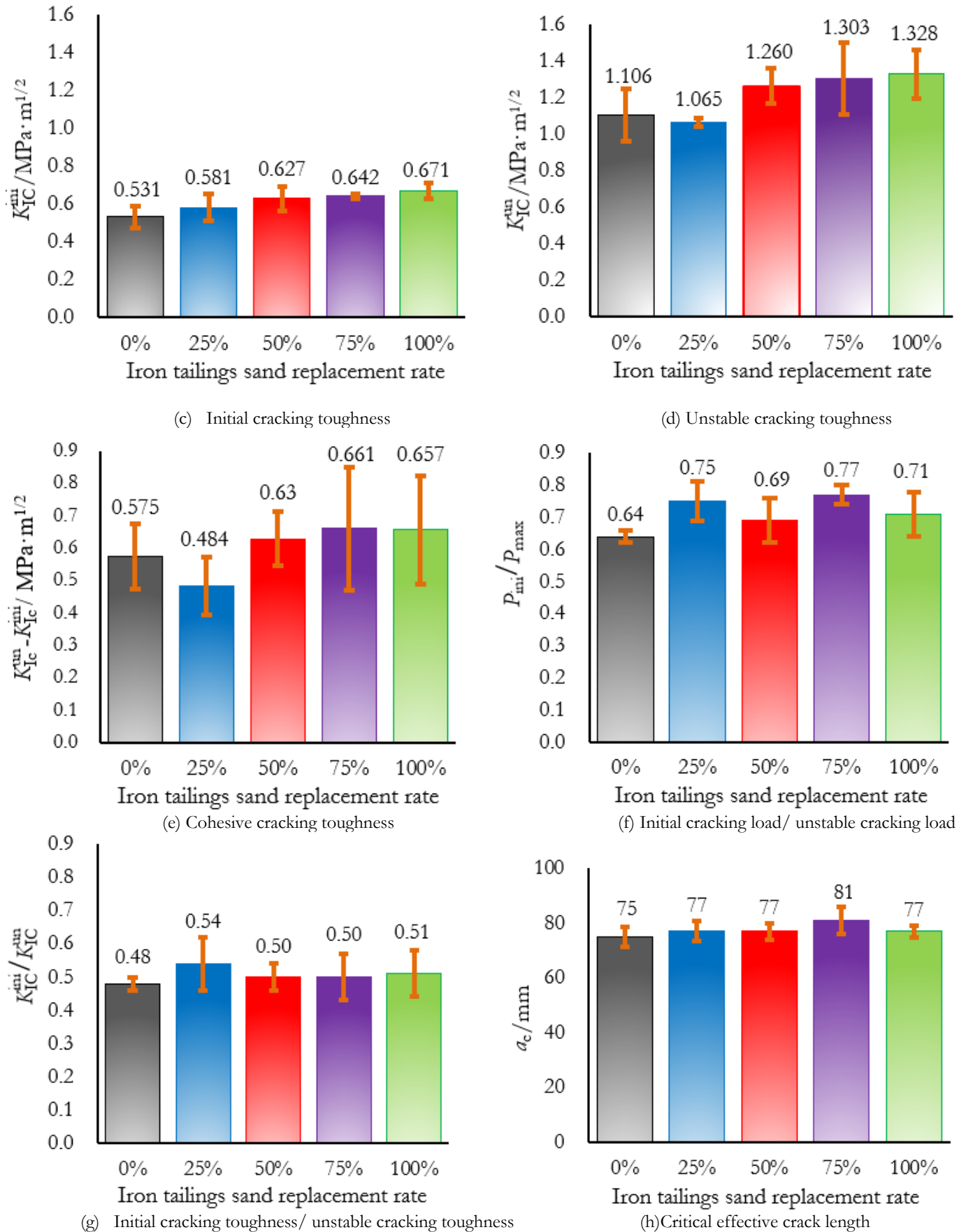


Figure 7: Relationship between fracture parameters and replacement rate.

As can be noticed from Fig. 7c, K_{IC}^{ini} increased by 26% from $0.531 \text{ MPa}\cdot\text{m}^{1/2}$ for river sand concrete to $0.671 \text{ MPa}\cdot\text{m}^{1/2}$ for 100% iron tailings sand concrete. As in Fig. 7d, K_{IC}^{un} showed some fluctuations, with the lowest K_{IC}^{un} for a 25% replacement rate and an increase in K_{IC}^{un} from 50% to 100% replacement rate. Overall, K_{IC}^{un} of the iron tailings sand concrete was not significantly lower than that of river sand concrete, and K_{IC}^{un} of the 100% replacement rate specimens increased by 20% compared to that of river sand concrete, which was less than K_{IC}^{ini} . For both P_{ini} and K_{IC}^{ini} , iron tailings sand concrete showed significant advantages. On the one hand, even though the water binder ratio of iron tailings sand concrete increased with the replacement rate during the mix design, it still showed a higher cubic compressive strength, indicating that iron tailings sand from ore crushing, which had a high iron content [3, 32], was more robust than river sand. On the other hand, iron tailings sand was more angular and irregular compared [3, 33] to river sand, with more contact points and a larger specific surface area, which enhanced the interfacial action of the slurry and fine aggregate during the hydration of cement, forming a more solid skeleton. Therefore, the iron tailings mortar was more dense, so P_{ini} and K_{IC}^{ini} were improved. The fluctuations in P_{max} and K_{IC}^{un} with replacement rate were mostly attributed to the non-uniform distribution of coarse aggregates. According to the double K fracture criterion, $K_{IC}^{un} - K_{IC}^{ini}$ (Fig. 7e) is the cohesive fracture toughness, which is generated by the cohesive stress on the fracture process zone and reflects the cohesive occlusion of aggregates and mortar. This value showed a roughly increasing trend with increasing replacement rate which also confirmed the previous deduction regarding a certain increase in the interfacial strength between mortar and coarse aggregate. Overall, the monotonically rising trend was not statistically significant, but the addition of adequate iron tailings sand improved the cohesive bond between the aggregates and mortar, leading to greater P_{max} and K_{IC}^{un} . Fig. 7f and 7g demonstrates the variable features of P_{ini} / P_{max} , and $K_{IC}^{ini} / K_{IC}^{un}$ in relation to the replacement rate. Compared to river sand concrete, the ratio of parameters increased with the addition of iron tailings sand, and the variation between the different replacement rates was not significant, indicating that the crack expansion process of river sand concrete specimens was smoother and more ductile than that of iron tailings sand concrete [34]. However, a_c represented the effective crack length when P_{max} was attained and also reflected the specimen's ductility to some degree. In general, the greater the value of a_c , the greater the ductility, which seems to contradict the conclusion drawn from the ratio of parameters stated previously. However, ductility regarding fracture is more primarily concerned with the capacity to maintain the crack's stable extension after crack initiation; therefore, the article evaluates ductility based on P_{ini} / P_{max} and $K_{IC}^{ini} / K_{IC}^{un}$ which is more in line with the definition of ductility. As a result, the addition of iron tailings sand reduced the material's ductility somewhat.

MICROSCOPIC TEST RESULTS AND DISCUSSION

Microstructure

Typically, the initial microcracks during concrete damage emerge first in the ITZ, hence the ITZ has a substantial impact on the macroscopic fracture characteristics of concrete [35]. The SEM images of specimens S0-1 and S4-4 are displayed in Fig. 8. Fig. 8a and 8c both depict ITZ sections enlarged 2000-3000 times, where the dense section was coarse aggregate, the light grey section was mortar and the black banded section was cracks. The iron tailings sand mortar (S4-4) had a relatively dense morphology, and in the river sand concrete, the coarse aggregate to mortar interface and cracking faults in the mortar were more apparent. Figs. 8b and 8d depict the results enlarged by a factor of 10,000. C-S-H gels with agglomerated flocs were more dense and homogenous in the iron tailings sand concrete, but ettringite rods were prevalent in the IZT of the river sand concrete, making the concrete more susceptible to cracking and fracturing under load. The iron tailings sand is characterized by its sharp angularity, which makes the combination with the cementitious matrix strong and flake-resistant [36], and, as seen in Fig. 2, the iron tailings sand had more fine particles, which can have a "micro-filling" effect and increase the denseness of the transition zone between the mortar and the interface [10]. In addition, the volcanic ash reaction of some of the iron tailings sand resulted in a more homogeneous microstructure [4]. Consequently, compared to river sand concrete, the ITZ of iron tailings sand concrete had a denser structure and a better state of sand-cement matrix bonding, making it more resistant to cracking, which explained the superior macrofracture capabilities of 100% replacement iron tailings sand concrete.

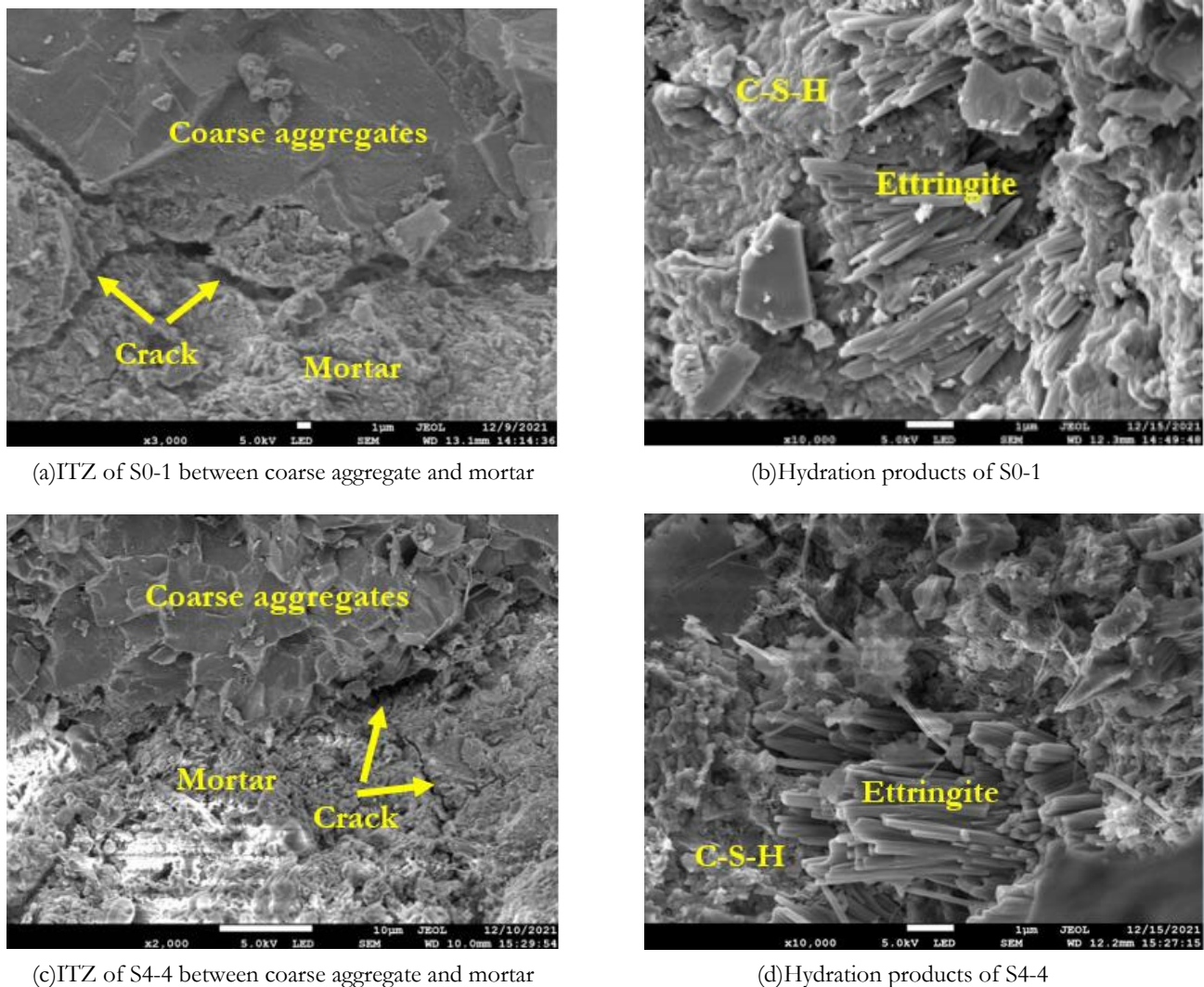


Figure 8: SEM images of S0-1 and S4-4

Pore structure

Pores are an essential component of concrete's microstructure and have a significant impact on the macroscopic characteristics of concrete. The porosity, average pore size, and pore size distribution obtained by mercury intrusion porosimetry are displayed in Tab. 4 below. As indicated in Tab. 4, the porosity has been reduced more dramatically with 75% and 100% iron tailings sand replacement. In general, the porosity is closely related to the compressive strength of the material, the general trend being that the porosity decreases and the compressive strength increases, so this result also explained the macroscopic law obtained in the cubic compressive test. The change in mean pore size was not significant. Wu, Z.W. [37] pointed out that <20nm is a harmless pore, 20-50 nm is a less harmful pore, 50-200nm is a harmful pore, and >200 nm is a more harmful pore based on the different impacts of different pore sizes on the performance of concrete. The proportion of more harmful pores in river sand concrete was 51.86% and the proportion of less harmful and harmless pores was 36.15%. The proportion of more harmful pores in iron tailings sand concrete was less than in river sand concrete, while the proportion of less harmful and harmless pores was generally high, but the degree of variation was not significant. If the more harmful pore holes > 200 nm are considered cracks or defects, along with the results of the microscopic morphology, it was possible that this portion of the harmful pore weakened the bond in the ITZ, causing river sand concrete to exhibit lower fracture toughness than iron tailings sand concrete in macroscopic tests. However, the results of the mercury intrusion porosimetry tests did not show strict agreement with the macroscopic tests. This is mostly owing to the fact that the performance of macroscopic mechanical qualities is influenced by microscopic morphology and phase composition, but is not dependent on pore structure. Overall, the addition of iron tailings sand enabled the concrete to be more compact, refining the pore size and reducing large pores while increasing small ones.



Sample	Porosity(by volume)/%	Average pore diameter/nm	Pore diameter distribution(by volume)/%			
			0-20nm	20-50nm	50-200nm	>200nm
S0	12.65(0.22)	43.46	18.94	17.21	11.99	51.86
S1	13.75(1.68)	44.52	18.33	20.93	9.95	50.79
S2	12.44(1.07)	46.66	16.03	22.49	15.01	46.47
S3	9.12(1.24)	43.03	17.34	20.12	14.97	47.57
S4	6.34(0.95)	46.88	17.82	21.80	12.45	47.93

Table 4: Pore diameter distribution(standard deviations in parentheses).

CONCLUSIONS

The P-CMOD curves of river sand concrete and iron tailings sand concrete exhibited the same trend, with no significant difference in the fracture process; the fracture surfaces of both types of concrete were uneven, the percentage of coarse aggregate fracture was comparable, and there was no significant difference in the damage pattern.

P_{ini} and K_{IC}^{ini} showed a clear trend of improvement with increasing replacement rate. P_{max} and K_{IC}^{un} of iron tailings sand concrete were generally greater than those of river sand concrete, but the improvement was not as large as P_{ini} and K_{IC}^{ini} , and the pattern of improvement displayed some fluctuations. Overall, the addition of iron tailings sand increased the material's resistance to initial and unstable cracking damage.

A comprehensive comparison of P_{ini} / P_{max} , $K_{IC}^{ini} / K_{IC}^{un}$ and a_c were assessed: the crack expansion process was smoother in river sand concrete, and the ductility of iron tailings sand concrete was slightly inferior to that of river sand concrete. The sharp angularity of the iron tailings sand made the combination with the cement matrix strong and resistant to flaking, and the microfilling effect and volcanic ash reaction made the microstructure denser and more uniform. The ITZ of iron tailings sand concrete was more resistant to cracking than river sand concrete. The proportion of more harmful pores in iron tailings sand concrete was lower than in river sand concrete, while the proportion of less harmful and harmless pores was generally high, but none of the variations were significant. The addition of iron tailings sand can made the concrete more dense, refined the pore size, reduced large pores and increased small pores.

ACKNOWLEDGMENTS

This researcher was funded by the National Natural Science Foundation of China (51378331), Tangshan Science and Technology Plan Project (20130224b), and Hebei Province Construction Science and Technology Research Project (2022-2162).

NOMENCLATURE

- L length of the specimen
- S the span between the two supports of the specimen
- H height of the specimen cross-section
- B thickness of the specimen cross-section
- a effective crack length
- a_0 initial notch crack length
- P load



CMOD	crack mouth opening displacement
P_{ini}	initial cracking load
P_{max}	unstable cracking load
ϵ	strain
K_I	fracture toughness
K_{IC}^{ini}	initial cracking toughness
K_{IC}^{un}	unstable cracking toughness
mg	mass between the specimen supports (converted from the total mass of the specimen by the S/L ratio)
g	gravitational acceleration
$CMOD_c$	crack mouth opening displacement corresponding to the unstable cracking load
a_c	critical effective crack length
E	elastic modulus, calculated by initial compliance of a P-CMOD curve
c_i	initial flexibility
H_0	thickness of holder of clip gauge
SEM	scanning electron microscopy
MIP	mercury intrusion porosimetry
ITZ	interface transition zone

REFERENCES

- [1] Lu, J. T., Kong, L.J., Fan, Z.R., Xie, S.H. (2022). Study on the interface and properties of iron tailings-geopolymer composites. *Journal of Building Materials*. 25(6), pp.585-606, DOI: 10.3969/j.issn.1007-9629.2022.06.006
- [2] Lu, C., H, M., Yang, J., Wang, Q., Tan, L., Fu, J. (2020). Utilization of iron tailings to prepare high-surface area mesoporous silica materials. *Science of the Total Environment*. 736, 139483. DOI: 10.1016/j.scitotenv.2020.139483.
- [3] Zhao, J.H., Ni, K., Su, Y.P., Shi, Y.X. (2021). An Evaluation of iron ore tailings characteristics and iron ore tailings concrete properties. *Construction and Building Materials*. 286, 122968. DOI: 10.1016/j.conbuildmat.2021.122968
- [4] Zhang, W.F., Gu, X.W., Qiu, J.P., Liu, J.P., Zhao, Y.Q., Li, X.H. (2020). Effects of iron ore tailings on the compressive strength and permeability of ultra-high performance concrete. *Construction and Building Materials*, 260, 119917, DOI: 10.1016/j.conbuildmat.2020.119917.
- [5] Liu, W. Y., Xu, X. L., An, Y. Y. (2011) Study on the sprayed concrete with iron tailings. *Advanced Materials Research*, 347–353, pp.1939–1943, DOI:10.4028/www.scientific.net/AMR.347-353.1939.
- [6] Zhang, G.D., Zhang, X.Z., Zhou, Z.H., Cheng, X. (2014) Preparation and properties of concrete containing iron tailings/manufactured sand as fine aggregate. *Advanced Materials Research*, 838, pp. 152–155 DOI: 10.4028/www.scientific.net/AMR.838-841.152.
- [7] Shettima, A.U., Hussin, M.W., Ahmad, Y., Mirza, J. (2016) Evaluation of iron ore tailings as replacement for fine aggregate in concrete. *Construction and Building Materials*, 120, pp. 72–79, DOI: 10.1016/j.conbuildmat.2016.05.095.
- [8] Tian, Z.X., Zhao, Z.H, Dai, C.Q., Liu, S.J. (2016) Experimental study on the properties of concrete mixed with iron ore tailings. *Advances in Materials Science and Engineering*. 2016, pp. 1–9, DOI: 10.1155/2016/8606505.
- [9] Bangalore Chinnappa, G., Karra, R. C. (2020) Experimental and statistical evaluations of strength properties of concrete with iron ore tailings as fine aggregate. *Journal of Hazardous, Toxic, and Radioactive Waste*, 24 (1), 04019038, DOI: 10.1061/(ASCE)HZ.2153-5515.0000480.
- [10] Zhu, Z.G., Li, B.X., Zhou, M.K. (2015) The Influences of Iron Ore Tailings as Fine Aggregate on the Strength of Ultra-High Performance Concrete. *Advances in Materials Science and Engineering*, 2015, pp. 1–6, DOI: 10.1155/2015/412878.
- [11] Slowik, M. (2021). The role of aggregate granulation on testing fracture properties of concrete. *Frattura ed Integrità Strutturale*, 15(58), pp. 376-385, DOI: 10.3221/IGF-ESIS.58.27.
- [12] Li, Q.B., Qing, L.B., Guan, J.F. (2012) Analysis of the whole fracture process of concrete considering effects of cohesive distribution. *Journal of Hydraulic Engineering*, 43, pp. 31-36, DOI: 10.13243/j.cnki.slxb.2012.s1.014.
- [13] Xu, S.L., Reinhardt, H. W. (1999) Determination of Double-K Criterion for Crack Propagation in Quasi-brittle Materials,



- Part II: Analytical Evaluating and Practical Measuring Methods for Three-point Bending Notched Beams. *International Journal of Fracture*, 98(2), pp. 151-177, DOI: 10.1023/A:1018740728458.
- [14] Xu, S.L., Reinhardt, H. W.(2000) A Simplified Method for Determining Double-K Fracture Parameters for Three-Point Bending Tests. *International Journal of Fracture*,104(2), pp. 181-209, DOI: 10.1023/A:1007676716549.
- [15] Ince, R. (2012)Determination of the fracture parameters of the double-K model using weight functions of split-tension specimens. *Engineering Fracture Mechanics*, 96(18), pp. 416-432, DOI:10.1016/j.engfracmech.2012.08.024.
- [16] Xu, S.L., Malik, M.A., Li, Q. H., Wu, Y. (2016)Determination of double-K fracture parameters using semi-circular bend test specimens. *Engineering Fracture Mechanics*, 152(2), pp. 58-71, DOI:10.1016/j.engfracmech.2015.12.006.
- [17] Kumar, S., Pandey, S.R., Srivastava, A. K. L.(2014) Determination of double-K fracture parameters of concrete using peak load method. *Engineering Fracture Mechanics*, 131, pp. 471-484, DOI:10.1016/j.engfracmech.2014.09.004
- [18] Qing, L.B., Li, Q.B. (2013)A theoretical method for determining initiation toughness based on experimental peak load. *Engineering Fracture Mechanics*,99, pp. 295-305, DOI:10.1016/j.engfracmech.2013.01.012.
- [19] Qing, L.B., Nie Y.T., Liu N., Guan J.F. (2016)Determination method for initial fracture toughness of dam concrete using linear regression. *Journal of Hydroelectric Engineering*, 35, pp. 25-31, DOI : 10.11660/slfdx.20160803.
- [20] Nie, Y.T, Qing, L.B. (2020)The Relationship between Double-K Parameters of Concrete Based on Fracture Extreme Theory. *Journal of Theoretical and Applied Mechanics*. 58 (1), pp. 59–71, DOI:10.15632/jtam-pl/115240.
- [21] Wu, Z.M., Xu, S.L., Liu, H.Y., Liu, Y. (2000)Influences of maximum aggregate sizes on double-K fracture parameters of concrete. *Journal of Dalian University Technology*, 40, pp. 358-361.
- [22] Qiu, P. (2019)Experimental Research on Fracture Behavior of Concrete after High Temperature. *Frattura ed Integrità Strutturale*, 13 (50), pp. 300–309, DOI: 10.3221/IGF-ESIS.50.25.
- [23] Xie, J., Liu, Y., Yan, M. L., Yan, J.B. (2022)Mode I Fracture Behaviors of Concrete at Low Temperatures. *Construction and Building Materials*, 323, 126612, DOI: 10.1016/j.conbuildmat.2022.126612.
- [24] Zhao, Y.H., Xu, S.L., Wu, Z.M. (2004)A dual G criterion for crack propagation in concrete structures. *China Civil Engineering Journal*, 37, pp. 13-18, DOI:10.15951/j.tmgcxb.2004.10.002.
- [25] Wu, Z.M., Dong, W., Liu, K., Yang, S.T. (2007)Mode I crack propagation criterion of concrete and numerical simulation on complete process of cracking. *Journal of Hydraulic Engineering*, 38, pp. 1453-1459, DOI:10.13243 /j.cnki.slx.2007.12.015.
- [26] Qin, Y.J., Chen, N., Lin, P.J., Yu, J. (2021)Double K fracture characteristics of recycled concrete three-point bending beam mixed with lithium slag. *Journal of Jilin University(Engineering and Technology Edition)*,51(06), pp.2121-2127, DOI: 10.13229/j.cnki.jdxbgxb.20200590.
- [27] Liang, N.H., Ren, L.X., Tian, S., Liu, X.R., Zhong, Z.L., Deng, Z.Y., Yan, R. (2021)Study on the fracture toughness of polypropylene–basalt fiber-reinforced concrete. *International Journal of Concrete Structures and Materials*, 15 (1), 35, DOI: 10.1186/s40069-021-00472-x.
- [28] MOHURD, JGJ52-2006,(2007).Standard for technical requirements and test method of sand and crushed stone (or gravel) for ordinary concrete. MOHURD, Beijing, China.
- [29] MOHURD, GB/T 50081-2019, (2019). Standard for test methods of concrete physical and mechanical properties. MOHURD, Beijing, China
- [30] NDRC, DL/T 5332-2005,(2006), Norm for fracture test of hydraulic concrete.. NDRC, Beijing, China.
- [31] Xu, S.L., Li, Q.H., Wu, Y., Dong, L.X., Lyu, Y., Reinhardt, H.W., Leung, C.K.Y., Ruiz, G., Kumar, S.; Hu, S.W.(2021). RILEM Standard: testing methods for determination of the double-K criterion for crack propagation in concrete using wedge-splitting tests and three-point bending beam tests, recommendation of RILEM TC265-TDK. *Materials and Structures*, 54(6), 220, DOI: 10.1617/s11527-021-01786-8.
- [32] Lv, X., Shen, W., Wang, L., Dong, Y., Zhang, J., Xie, Z.(2019). A comparative study on the practical utilization of iron tailings as a complete replacement of normal aggregates in dam concrete with different gradation. *Journal of Cleaner Production* 211, pp. 704–715. DOI: 10.1016/j.jclepro.2018.11.107
- [33] Yang, Y.H., Wei Z.A., Chen, Y.L., Ren, B.X.(2017). Study on the shapes of tailings particles based on microscopy and image processing technologies. *Chinese Journal of Rock Mechanics and Engineering*,36(supp1), pp. 3689-3695. DOI: 10.13722/j.cnki.jrme.2016.0594.
- [34] Han,Y.D., Wang,Z.B.,Liu W.K.,Yue,Q.R., Ding,X.P.(2021). Comparative study on fracture properties of seawater coral aggregate concrete with different strengths. *Journal of Building Materials*, 24(04), pp.881-886. DOI: 10. 3969/j.issn.1007-9629.2021.04.028
- [35] Xu, F., Wang, S.L., Li, T., Liu, B., Li, B.B., Zhou, Y. (2021)Mechanical properties and pore structure of recycled aggregate concrete made with iron ore tailings and polypropylene fibers. *Journal of Building Engineering*, 33, 101572, DOI: 10.1016/j.job.2020.101572.



- [36] Lv, X.D., Lin, Y.Q., Chen, X., Shi, Y., Liang, R.Q., Wang, R.K., Peng, Z.L. (2021) Environmental impact, durability performance, and interfacial transition zone of iron ore tailings utilized as dam concrete aggregates. *Journal of Cleaner Production*, 292, 126068, DOI: 10.1016/j.jclepro.2021.126068.
- [37] Yu, L.(2017) *Micro-properties of cement concrete*, China Architecture Publishing & Media Co.Ltd, Beijing.